

# Detailed Hydration Maps of Benzene and Cyclohexane Reveal Distinct Water Structures

Tanya M. Raschke\* and Michael Levitt

Department of Structural Biology, Fairchild Building, Room D-100, Stanford University,  
Stanford, California 94305

Received: February 5, 2004; In Final Form: May 20, 2004

The hydration structures of the hydrophobic solutes benzene and cyclohexane were investigated using molecular dynamics (MD) simulations of a single solute in water. Detailed, spatially resolved, three-dimensional maps of the density of the water O and H atoms surrounding either benzene or cyclohexane were generated from the simulation data. MD simulations were computed for each solute using either the ENCAD or GROMACS program package and one of five distinct water models: F3C, TIP3P, TIP4P, SPC, or SPC/E. For each solute, five 100 ns data sets, each representing a unique simulation condition, were analyzed. The water structure maps generated from the five data sets for each solute are remarkably similar. Our results show that water molecules in the first hydration shell around cyclohexane bind weakly. In contrast, water molecules bind more strongly and in a hydrogen-bonding orientation to the faces of the benzene ring. The high-resolution maps of the water structure surrounding benzene and cyclohexane presented in this paper reveal details of the positional preferences of water not resolved by other methods. They also show that the hydration structure at this level of detail is remarkably insensitive to the potential energy functions and simulation methods used.

## Introduction

The hydrophobic effect is considered one of the most important driving forces in the stabilization of biological structures. Both the preferential solvation of polar groups in water along with the tendency of water to exclude apolar groups play a key role in the stabilization of protein native states,<sup>1</sup> macromolecular complexes, and membrane assembly.<sup>2,3</sup> The energetics of insertion of a nonpolar solute into water show a positive free energy, a positive entropy at room temperature, and a large, positive heat capacity.<sup>4–6</sup> The physical origins of these hallmarks of the hydrophobic effect, however, remain under debate. The strong hydrogen bonding interactions in water and the tendency of water to reorganize around a nonpolar solute to maintain these interactions are a possible source of the hydrophobic effect.<sup>4,7</sup> A more recent idea is that the small size of water molecules is the source of the unfavorable energetics.<sup>8–11</sup> Many studies have shown that the major contribution to the hydrophobic effect comes from creating a cavity in the solvent large enough to accommodate the solute. This observation is often applied to proteins and other macromolecules by relating hydration energy or hydrophobic interactions to the surface area of the solute.<sup>12–14</sup> This approach is a reasonable approximation for short, linear alkanes, but cyclic and branched solutes deviate from this simple behavior in ways that are difficult to predict.<sup>15</sup> Furthermore, conformational changes in longer alkanes have significant effects on the solvation energy.<sup>16</sup>

In an effort to better understand the hydration structures of cyclic hydrocarbons, we have investigated the detailed structure of water molecules surrounding benzene and cyclohexane as observed in molecular dynamics (MD) simulations. The solute and water molecules were modeled classically in our simulations. That is, each atom has a van der Waals radius and partial

charge. This representation of the solute molecules is more realistic than the often-studied, primitive, hard sphere models (see ref 17 for a recent review) yet are not as computationally expensive as models that include polarizability or full quantum mechanical representations.

One solute we have chosen to study is benzene, an example of a “hydrophobic” solute with important solute–solvent interactions. The aromatic structure of benzene imparts a negative partial charge on its faces and a positive partial charge around its edges. Benzene is an important solute model in that it is a key component of the amino acid phenylalanine and can serve as a simplified model for the aromatic structures of tyrosine, tryptophan, and the bases of nucleic acids. The ability of benzene to act as a hydrogen bond acceptor was predicted in the 1980s.<sup>18,19</sup> Since that time, experiments have shown that benzene does indeed form hydrogen bonds with water (ref 20 and references therein). Details of the water–benzene interaction have been investigated using Monte Carlo<sup>21,22</sup> and MD<sup>23,24</sup> simulations of a single benzene molecule in solution. These theoretical studies also show that water molecules prefer to adopt a hydrogen-bonding interaction with the faces of the benzene ring. This result is used to explain the higher relative solubility of benzene over that of other hydrocarbons.

To better discern the effects of aromaticity on hydration structure, we have also chosen to study the interaction of water with cyclohexane. Cyclohexane is similar to benzene in that it contains six cyclically arranged carbon atoms. It differs in its lack of aromaticity and has a somewhat less constrained structure. The surface area of cyclohexane (200.90 Å<sup>2</sup> solvent accessible surface area<sup>25</sup>) is very similar to that of benzene (192.70 Å<sup>2</sup>), and both molecules have an oblate shape. By comparing the arrangement of water molecules around these two solutes, the effects of the charge distribution of the solute on the water structure can be separated from effects caused by the shape of the solute.

\* Corresponding author. Phone: 650-725-0754. Fax: 650-723-8464. E-mail: raschke@stanford.edu.

**TABLE 1: MD Simulation Parameters and Water Models**

simulation name	program	water model	potential energy function <sup>a</sup>	electrostatics	simulation ensemble	total simulation time in ns (runs)	temperature (K)
ENCAD	ENCAD	F3C	ENCAD	cutoff <sup>b</sup>	NVE <sup>d</sup>	100 (10)	300
TIP4P	GROMACS	TIP4P	OPLS	PME <sup>c</sup>	NPT <sup>e</sup>	100 (10)	300
TIP3P	GROMACS	TIP3P	OPLS	PME	NPT	100 (10)	300
SPC	GROMACS	SPC	OPLS	PME	NPT	100 (10)	300
SPC/E	GROMACS	SPC/E	OPLS	PME	NPT	100 (10)	300

<sup>a</sup> The potential energy function is used for the hydrocarbon atoms. See Table 2 for details of the nonbonded interaction potentials. <sup>b</sup> Cutoff means that the energy for all nonbonded interactions (van der Waals and electrostatics) diminishes smoothly to zero at 6 Å. <sup>c</sup> PME is Particle Mesh Ewald, a method that computes electrostatics to infinite range. <sup>d</sup> NVE means constant number of molecules, volume, and energy. The water density was set to 1.0 g/mL. <sup>e</sup> NPT means constant number of molecules, pressure, and temperature. The pressure was set to 1 atm.

In this paper, we present a thermodynamic view of the time-averaged water structure surrounding two simple, hydrocarbon solutes: benzene and cyclohexane. Our approach is to use MD simulations to sample many configurations of water molecules around a solute and then generate three-dimensional (3-D) maps of the O and H atom positions. A similar approach was taken in mapping the 3-D water density surrounding a single water molecule.<sup>26,27</sup> Kusalik and Svishechev computed spatial distribution functions, akin to traditional, rotationally averaged, radial distribution functions, but dependent on both the radial and angular coordinates of the surrounding water molecules. These spatial maps not only showed the expected tetrahedral coordination of surrounding water molecules but also revealed maxima at interstitial positions. These interstitial maxima are not resolved in the angle-averaged radial distribution functions yet have important implications to the hydrogen-bonding pattern of water. Another advantage of this method is that it can be applied to irregularly shaped solutes easily. In this work, we show that this high-resolution approach to mapping the solvation structure of benzene and cyclohexane avoids spatial averaging and reveals structural details not resolved by other methods.

In addition, we compare the results of simulations computed using five different water models: F3C,<sup>28</sup> SPC,<sup>29</sup> SPC/E,<sup>30</sup> TIP3P,<sup>31</sup> and TIP4P.<sup>31</sup> Each of these models has been parametrized independently to reproduce various properties of bulk water, typically the density, diffusion constant, tetrahedral structure, dimerization energy, and pressure. In addition, each model has been extensively used in previous biomolecular simulations because of their relatively low computational cost. F3C, SPC, SPC/E, and TIP3P are all 3-point models, whereas TIP4P is a 4-point model. F3C is unique in that it is a fully flexible representation, while the other models are held at fixed bond lengths and angles. Two different MD programs, ENCAD<sup>32</sup> and GROMACS,<sup>33</sup> were used to compute the trajectories. The energetic parameters for the solute models were either the ENCAD potential or the OPLS potential.<sup>34</sup> We were curious to see the differences in hydration structure between the different models and simulation conditions. Surprisingly, the 3-D water structure maps constructed from each of these simulation sets all show very similar distributions, giving us confidence that these maps reflect the basic properties of water and are not dependent on the specific details of the individual models used.

The detailed hydration maps show that the water structure around benzene and cyclohexane is nonuniform and that water molecules preferentially occupy the interstices (between H atoms and along C–C bonds) on the surface of the solutes. Furthermore, our results show that water has a relatively strong, preferential interaction with the faces of the benzene molecule as shown by high O and H density. Interestingly, the waters located along the edges of the benzene do not interact as strongly with the solute. Water molecules in the first hydration shell of

cyclohexane behave similarly to those around the edge of the benzene ring.

## Computational Methods

**A. MD Simulations.** Molecular dynamics (MD) simulations were computed using either the ENCAD or GROMACS program package. Each simulation consisted of a single solute, either benzene or the chair conformation of cyclohexane in a box of more than 2000 explicit water molecules. Interconversion between the boat and chair conformations of cyclohexane occurs on the order of microseconds, and no incidences of interconversion were observed in the simulations reported here. The largest observed fluctuations of the cyclohexane molecule resulted in conformations approaching that of the half-chair. The simulated systems were computed in a relatively large box to avoid problems with boundary conditions and to allow for an excess of water molecules and with long simulation times to ensure adequate sampling. The simulation box used for each simulation was cubic, had a side length of 40 Å, and was repeated using periodic boundary conditions.<sup>35</sup> A set of ten 10 ns simulations was computed for each set of conditions, for a total of 100 ns of simulation time. Each simulation differed in the seed for the random generator used to assign initial velocities. All simulations were computed at 300 K, with time step of 0.002 ps, and coordinates were stored every 1000 steps, or 2 ps. The first 500 ps of data were not used in the subsequent analysis, to allow sufficient equilibration of the system. The different sets of simulation conditions are summarized in Table 1.

The ENCAD simulations were run in the NVE ensemble using the standard ENCAD potential<sup>36</sup> (NVE means constant number of molecules, volume, and energy). A short, smoothly truncated cutoff of 6.0 Å was used for the nonbonded interactions (van der Waals and electrostatics). The water model used for the ENCAD simulations was the flexible, three-centered (F3C) water model.<sup>28</sup> A summary of the nonbonded energy and geometric parameters for F3C is given in Table 2, and the solute and solute–water parameters are given in Table 3. The solute was inserted into the box of solvent molecules, overlapping waters were removed, and the box dimensions were adjusted to obtain the proper water density of 1.0 g/mL. The system was minimized with 2000 steps of conjugate gradient minimization before starting the dynamics simulation. Equilibration of the temperature to the desired value of 300 K was carried out in increments of 2 degrees.

The GROMACS simulations were run in the NPT ensemble using the OPLS potential energy parameters.<sup>34</sup> (NPT means constant number of molecules, pressure and temperature). Summaries of important nonbonded energy parameters for the solvent and solute are given in Tables 2 and 3. The solute was placed in a 40 Å cubic box of water molecules (represented by

**TABLE 2: Nonbonded Energy Parameters and Geometric Properties of the ENCAD<sup>a</sup> and GROMACS<sup>b</sup> Water Models**

parameter and units	F3C <sup>d</sup>	SPC <sup>e</sup>	SPC/E <sup>e</sup>	TIP3P <sup>e</sup>	TIP4P <sup>e</sup>
$\sigma^O$ (Å)	3.5532	3.16549	3.16549	3.15061	3.15365
$\epsilon^O$ (kcal mol <sup>-1</sup> )	0.1848	0.1554	0.1554	0.1521	0.1550
$A^{OO}$ (kcal Å <sup>12</sup> mol <sup>-1</sup> ) <sup>c</sup>	628 662	629 220	629 220	582 003	600 003
$B^{OO}$ (kcal Å <sup>6</sup> mol <sup>-1</sup> ) <sup>c</sup>	743.79	625.40	625.40	595.06	609.92
$\sigma^H$ (Å)	0.9000	0	0	0	0
$\epsilon^H$ (kcal mol <sup>-1</sup> )	0.0100	0	0	0	0
$A^{HH}$ (kcal Å <sup>12</sup> mol <sup>-1</sup> ) <sup>c</sup>	0.0024	0	0	0	0
$B^{HH}$ (kcal Å <sup>6</sup> mol <sup>-1</sup> ) <sup>c</sup>	0.0106	0	0	0	0
$q^O$ (e)	-0.820	-0.820	-0.8476	-0.834	0
$q^H$ (e)	0.410	0.410	0.4238	0.417	0.520
$q^W$ (e)	0	0	0	0	-1.040
$r_0^{OH}$ (Å)	1.0000	1.0000	1.0000	0.9572	0.9572
$\angle HOH$ (deg)	109.47	109.47	109.47	104.52	104.52

<sup>a</sup> In the ENCAD simulations, the Lennard-Jones energy function is

$$V_{LJ}(r_{ij}) = A_{sc}\epsilon_{ij}\left(\frac{\sigma_{ij}}{r_{ij}}\right)^{12} - 2\epsilon_{ij}\left(\frac{\sigma_{ij}}{r_{ij}}\right)^6 - S_{LJ}(r_{ij})$$

where  $r_{ij}$  is the distance between atoms  $i$  and  $j$ . Both  $\sigma_{ij}$  and  $\epsilon_{ij}$  are calculated as the geometric mean of the atom-type specific  $\sigma_{ii}$  and  $\epsilon_{ii}$  parameters.  $A_{sc}$  reduces the repulsive Lennard-Jones energy to compensate for attractive interactions lost by using a short cutoff distance,  $r_c = 6.0$  Å. The value of  $A_{sc}$  used was 0.84. The Lennard-Jones truncation shift function,  $S_{LJ}(r_{ij})$  is given by

$$S_{LJ}(r_{ij}) = \left[ A_{sc}\epsilon_{ij}\left(\frac{\sigma_{ij}}{r_c}\right)^{12} - 2\epsilon_{ij}\left(\frac{\sigma_{ij}}{r_c}\right)^6 \right] - \frac{12(r_{ij} - r_c)}{r_c} \left[ A_{sc}\epsilon_{ij}\left(\frac{\sigma_{ij}}{r_c}\right)^{12} - \epsilon_{ij}\left(\frac{\sigma_{ij}}{r_c}\right)^6 \right]$$

and is applied to  $r_{ij}$  less than the cutoff value,  $r_c$ . The Coulombic energy function in the ENCAD simulations is given by the function

$$V_C(r_{ij}) = f \left( \frac{q_i q_j}{r_{ij}} - S_C(r_{ij}) \right)$$

where  $f = 1/4\pi\epsilon_0 = 332.06$  kcal mol<sup>-1</sup> nm Å e<sup>-2</sup> is the factor for converting the electric quantity to a mechanical one. The Coulombic truncation shift function,  $S_C(r_{ij})$ , is given by

$$S_C(r_{ij}) = \left[ \frac{q_i q_j}{r_c} \right] - (r_{ij} - r_c) \left[ \frac{q_i q_j}{r_c^2} \right]$$

<sup>b</sup> In the GROMACS simulations, the Lennard-Jones energy function is

$$V_{LJ}(r_{ij}) = 4\epsilon_{ij} \left[ \left( \frac{\sigma_{ij}}{r_{ij}} \right)^{12} - \left( \frac{\sigma_{ij}}{r_{ij}} \right)^6 \right]$$

$\sigma_{ij}$  is calculated as the arithmetic mean of the atom-type specific  $\sigma_{ii}$  parameters, while  $\epsilon_{ij}$  is calculated as the geometric mean of the  $\epsilon_{ii}$  parameters. The Coulombic energy function for the Gromacs simulations is

$$V_C(r_{ij}) = f \frac{q_i q_j}{r_{ij}}$$

with the value for  $f$  as described above. <sup>c</sup> For the ENCAD simulations, the repulsive Lennard-Jones parameter,  $A$ , is calculated as  $A_{sc}\epsilon_{ij}\sigma_{ij}^{12}$ , and the attractive parameter,  $B$ , as  $-2\epsilon_{ij}\sigma_{ij}^6$ . For the GROMACS simulations,  $A$  is calculated as  $4\epsilon_{ij}\sigma_{ij}^{12}$ , while  $B$  is  $4\epsilon_{ij}\sigma_{ij}^6$ . <sup>d</sup> The F3C water model in the ENCAD simulations is flexible and includes Lennard-Jones interactions on the H atoms as well as the O. <sup>e</sup> All of the water models used in GROMACS (SPC, SPC/E, TIP3P, TIP4P) were restrained to fixed bond lengths and angles in the simulations.

either the SPC, SPC/E, TIP3P, or TIP4P water model), and the system was minimized using 250 steps of steepest descent minimization. The box was equilibrated with a short MD simulation of 100 000 steps with a step size of 0.001 ps. A cutoff of 14 Å was used for the van der Waals interactions, and the Particle Mesh Ewald (PME) summation<sup>37</sup> was used for the

**TABLE 3: Nonbonded Energy Parameters<sup>a</sup> for the Solute and Solute–Water Interactions in ENCAD and GROMACS**

parameter and units	ENCAD/F3C		GROMACS/TIP4P	
	benzene	cyclohexane	benzene	cyclohexane
$\sigma^C$ (Å)	4.2202	4.3150	3.5500	3.1536
$\epsilon^C$ (kcal mol <sup>-1</sup> )	0.0376	0.0738	0.0700	0.0660
$\sigma^H$ (Å)	2.8525	2.8525	2.4200	2.5000
$\epsilon^H$ (kcal mol <sup>-1</sup> )	0.0380	0.0380	0.0300	0.0300
$A^{CO}$ (kcal Å <sup>12</sup> mol <sup>-1</sup> ) <sup>b</sup>	796 367	1 274 442	837 820	743 630
$B^{CO}$ (kcal Å <sup>6</sup> mol <sup>-1</sup> ) <sup>b</sup>	562.35	841.92	590.83	548.50
$A^{HO}$ (kcal Å <sup>12</sup> mol <sup>-1</sup> ) <sup>b</sup>	76 312	76 312	59 855	71 019
$B^{HO}$ (kcal Å <sup>6</sup> mol <sup>-1</sup> ) <sup>b</sup>	174.50	174.50	127.77	139.18
$A^{CH}$ (kcal Å <sup>12</sup> mol <sup>-1</sup> ) <sup>b</sup>	48.92	78.29	0	0
$B^{CH}$ (kcal Å <sup>6</sup> mol <sup>-1</sup> ) <sup>b</sup>	2.12	3.18	0	0
$A^{HH}$ (kcal Å <sup>12</sup> mol <sup>-1</sup> ) <sup>b</sup>	4.69	4.69	0	0
$B^{HH}$ (kcal Å <sup>6</sup> mol <sup>-1</sup> ) <sup>b</sup>	0.66	0.66	0	0
$q^C$ (e)	-0.119	-0.238	-0.115	-0.120
$q^H$ (e)	0.119	0.119	0.115	0.060

<sup>a</sup> See Table 2 for a description of the energy functions used in the simulations. <sup>b</sup> The Lennard-Jones attractive parameter,  $A$ , and the repulsive parameter,  $B$ , were calculated as described in Table 1. The parameters shown here are for solute–solvent interactions, for instance,  $A^{CO}$  is the value for the solute C to water O interaction. For the ENCAD simulations, the water model was F3C and the solute potential was ENCAD. For GROMACS, the data shown are for the TIP4P water model and the OPLS solute potential.

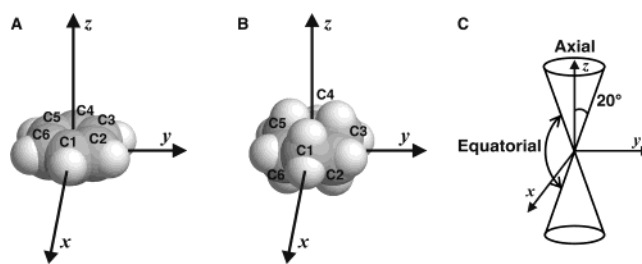


**Figure 1.** Geometric descriptions of reference axes and axial and equatorial volume regions. (A) Orientation of benzene on the reference axes. (B) Orientation of cyclohexane on the reference axes. In both cases, the solute centroid is positioned at the origin, the  $x$ -axis passes through atom C1, and the  $y$ -axis bisects the C2–C3 bond. The  $z$ -axis lies along the 6-fold rotation axis of benzene and the 3-fold rotation axis of cyclohexane. (C) The axial volume region surrounding the solute is defined by the volume of the cones circumscribed by vectors starting at the origin and lying 20° from the positive and negative  $z$ -axis. The remaining volume is considered to be the equatorial region.

electrostatic interactions. The Berendsen method<sup>38</sup> was used for both pressure and temperature coupling. The time interval between output coordinates was identical to that of the ENCAD simulations.

**B. 3-D Mapping of the Water Density Surrounding the Solutes.** The locations of the water molecules surrounding either the cyclohexane or benzene solute were mapped using a method similar to that of Kusalik and Svischev.<sup>26,27</sup> Instead of mapping into spherical coordinate space, however, we mapped the positions of the water atom centers (either O or H) into Cartesian space, which can be used for solutes of arbitrary shape and has the added advantage of uniformly sized volume elements. The positions of the water molecules surrounding the solute were collected and summed over each set of 10 runs. At each time step, the simulation box was centered on the centroid of the solute, and the system was rotated onto the reference axes using the method of MacLachlan<sup>39</sup> (i.e. by minimizing the root-mean-square deviation of the positions of the carbon atoms with that of a properly oriented molecule). Figure 1A,B illustrates the orientations of the benzene and cyclohexane solutes on the reference axes.



The positions of the O and H atom centers for each water molecule that fell within a 20 Å box, defined by (*x,y,z*) coordinates within −10 and 10 Å, were placed into 3-D histograms with 80 bins in each dimension, corresponding to a bin width of 0.25 Å. The densities of the water O and H atoms were tabulated separately. The number of water atoms in each bin was normalized by dividing by the average number of water atoms observed within the volume of a single element in an identical simulation that contained only water. This value was taken to be the reference or bulk density.

**C. Calculation of Spatially Averaged Radial Distribution Functions.** The spatially averaged solute centroid to water atom radial distribution functions,  $g_{\text{Sol-O}}$  and  $g_{\text{Sol-H}}$ , of the water density surrounding the solutes were computed separately using polar coordinates, as spherical averaging of gridded data introduces noise into the distributions. When computing the radial distribution functions, the simulation box at each time step was centered and oriented relative to the solute molecule as described above. Water molecule atoms whose center fell within  $r \leq 10$  Å from the solute centroid were included. Due to the nonspherical nature of benzene and cyclohexane, the  $g_{\text{Sol-O}}$  and  $g_{\text{Sol-H}}$  were computed separately for two volume regions, termed the axial and equatorial regions.<sup>21</sup> The axial region was defined as the volume of the cones swept out by vectors 20° from the positive and negative *z*-axis. Water molecules whose oxygen centers that fell outside of that volume were considered in the equatorial region (see Figure 1C). The radial distribution functions were computed in the usual fashion,<sup>35</sup> using a bin width,  $\Delta r$ , of 0.05 Å.

The solvent–solute dimerization energy is manifest in the  $g_{\text{Sol-O}}$ . To illustrate this, we calculate a “potential of mean force”, *PMF*, which represents the free energy of a water molecule at various distances from the solute, relative to that at infinite separation from the solute (i.e. a water molecule in the bulk). *PMF* is related to  $g_{\text{Sol-O}}$  by eq 1

$$PMF(r) = -RT \ln(g_{\text{Sol-O}}(r)) \quad (1)$$

where *T* is the temperature and *R* is the gas constant.

## Results

To gain some insight into the hydrophobic effect, we investigated the water structure surrounding the cyclic hydrophobic solutes benzene and cyclohexane. The results we report are time-averaged, but spatially resolved maps of water location obtained from five different sets of molecular dynamics simulations. The Results section of this paper is organized as follows: First, we present the detailed 3-D hydration maps of the location of the water molecules surrounding benzene and cyclohexane. Second, we compare the hydration maps computed from the five different sets of simulation conditions. Third, we present more traditional, rotationally averaged, radial distribution functions of the same positional data. Finally, *PMF* for water binding to the respective solute molecules are shown.

**A. Detailed Maps of the Hydration Structure of Benzene and Cyclohexane.** The computations described above generated detailed, 3-D maps of the water density surrounding a single benzene or cyclohexane molecule in water. Slices from representative water density maps surrounding each solute are shown in Figures 2 and 3. These data were taken from the ENCAD simulation sets and have not been rotationally averaged. The water O and H densities,  $\rho_{\text{O}}$  and  $\rho_{\text{H}}$ , have been normalized relative to that of bulk water ( $\rho = 1.0$ , gray contours) as determined by a water-only simulation under identical condi-

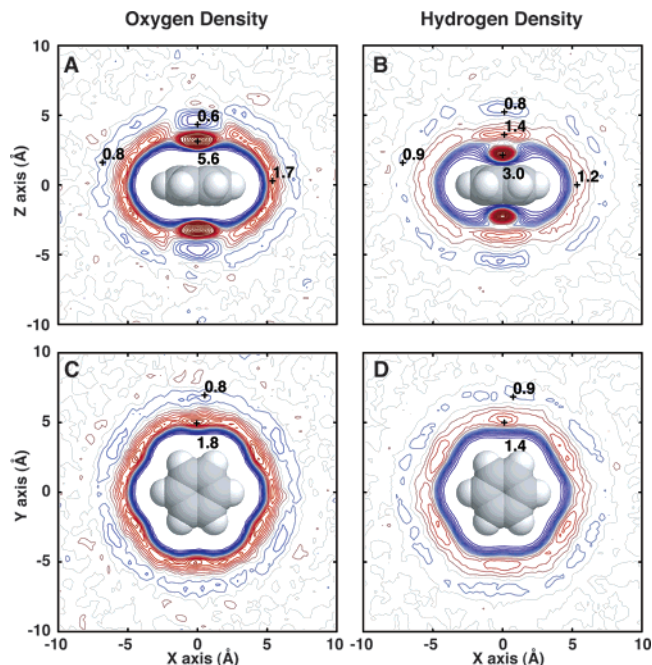


**Figure 2.** Water O and H density surrounding benzene. Slices through the 3-D water density maps from the benzene ENCAD simulations are shown. (A, C) Slices through the water O density map: the *xz*-plane (*y* = 0) and the *xy*-plane (*z* = 0), respectively. (B, D) The same slices through the water H density map. Contours represent the water atom (O or H) density values ( $\rho_{\text{O}}$  or  $\rho_{\text{H}}$ ) scaled relative to the atom density in bulk water,  $\rho = 1.0$ , and are drawn every 0.1 unit. Red and blue indicate high and low water density, respectively. The data were smoothed using a 3-D box average.

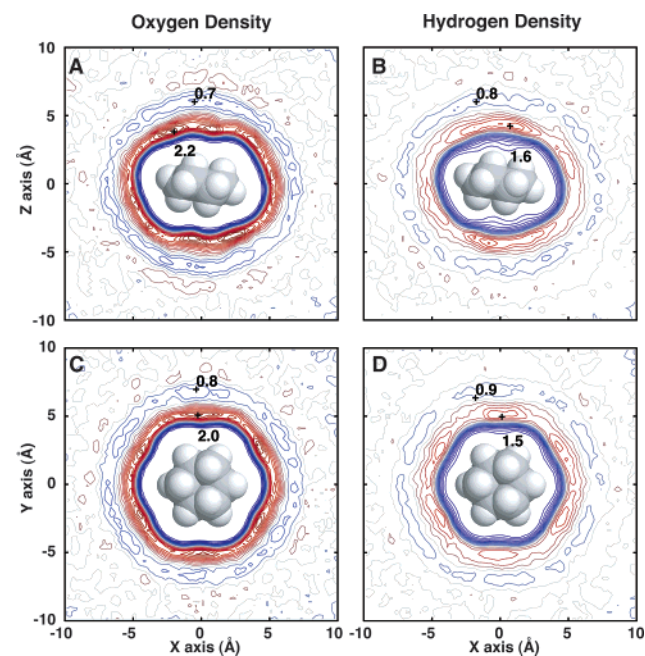


**Figure 3.** Water O and H density surrounding cyclohexane. Slices through the 3-D water density maps from the cyclohexane ENCAD simulations are shown. Slices and contours are identical to those in Figure 2. (A, C) Slices through the water O density map. (B, D) The same slices through the water H density map.

tions. There are several common features of the density maps for both solutes. These include the excluded solute volume, a well-defined first hydration shell (the volume including the innermost blue contours and the band of red contours), and the surrounding minimum density region (the second layer of blue contours). A less well-defined second hydration shell can also

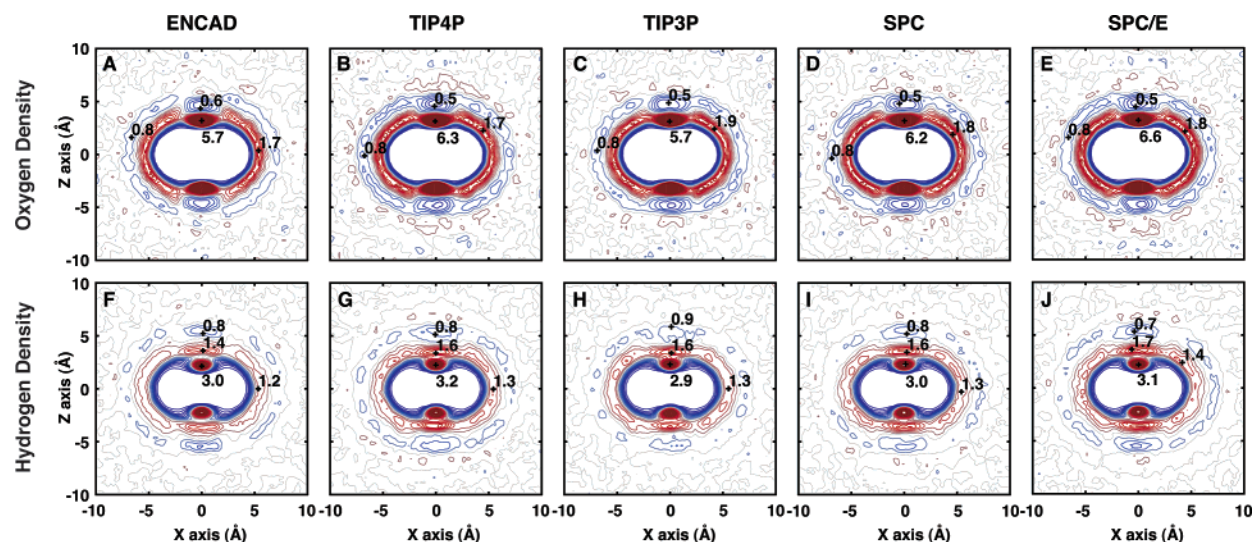


**Figure 4.** The water density maps around benzene for different water models and simulation conditions are essentially identical. Slices through the 3-D water O and H density maps computed from all five sets of simulation conditions are shown. Panels (A, B, C, D, E) show slices (as in Figure 2A) of the water O density maps computed from the ENCAD, TIP4P, TIP3P, SPC, and SPC/E simulations, respectively. The simulation conditions are described in Table 1. Panels (F, G, H, I, J) show slices of the water H density maps (as in Figure 2C) for the same five simulation conditions. The contour intervals and coloring are identical to those used in Figure 2.

be observed as regions of  $\rho > 1.0$ . At the edges of the grid box, the average water density varies slightly around that of bulk water (within  $\pm 0.1$ ), indicating the precision of the maps.

Although benzene and cyclohexane are similar in size (192.70 Å<sup>2</sup> and 200.90 Å<sup>2</sup> solvent accessible surface area, respectively) and shape, the water density surrounding these solute molecules is clearly different (Figures 2 and 3). Since the majority of the mass of a water molecule is located in the O atom, the O density maps illustrate the average water positions in the simulations. The corresponding H maps give insight into the orientation preferences of water at different locations surrounding the solute. Key features of the water density maps for cyclohexane and benzene are discussed below.

The most noticeable features of the benzene O density maps are two very prominent peaks located just above and below the plane of the benzene ring (Figure 2A). These peaks are centered 3.18 Å from the benzene centroid, have  $\rho_O = 5.6$  times bulk water density, and a combined volume of about 5 Å<sup>3</sup> (with  $\rho_O > 2.0$ ). The observation of these peaks indicates a favorable interaction with water, presumably with the localized negative charge along the benzene faces. This is further confirmed by the H density map (Figure 2B), which shows highly localized H density precisely between the benzene center and O density peak ( $\rho_H = 3.0$  at 2.23 Å). Combining both the O and H density results indicates that there is a strong preference for one water molecule to bind to each face of the benzene ring. The preferred orientation is with a single O–H bond collinear with the *z*-axis but maintaining rotational freedom as shown by the disc-shaped secondary peaks in the H density ( $\rho_H = 1.4$  at 3.68 Å) just beyond the global maxima. Due to the high water occupancy at these axial peaks, water molecules are excluded from the adjacent volume, and strong minima are observed in the O density at 4.6 Å with  $\rho_O = 0.6$  and in the H density at 5.4 Å and  $\rho_H = 0.8$ .

The water O density in the first hydration shell around the edge of the benzene molecule is more evenly distributed (Figure 2C), with a maximum  $\rho_O = 1.8$ , and occurs as a roughly ring-shaped band about 5 Å from the benzene centroid. Closer examination shows that the water density in this region is not completely uniform, but slightly higher density is found in the indented regions between the H atoms and along the C–C

bonds. A similar pattern is seen in the H density (Figure 2D). Overall, the H density shows a somewhat closer approach to the solute due to the weaker Lennard-Jones repulsions and less intensity in the first hydration shell than the O density.

The water O and H density maps for cyclohexane (Figure 3) do not show the strong peaks seen in the benzene maps. Rather, the water density in the first hydration shell is similarly distributed in both the axial (Figure 3A) and equatorial (Figure 3B) regions. The  $\rho_O$  and  $\rho_H$  show slightly higher intensity in a broadened cap in the axial region, but this effect is subtle. Most remarkably, both the O and H density in the equatorial region around cyclohexane are very similar to the same region surrounding benzene (Figure 2C,D). Once again, small density peaks are seen along the C–C bonds with maximum  $\rho_O = 1.9$  and  $\rho_H = 1.4$ , respectively. A relatively uniform, low-density region surrounds the first hydration shell, and a hint of a second shell can be seen in the O data (Figure 3A,C). Overall, the first hydration shell of cyclohexane is similar to that observed in the equatorial region of benzene, but the highly favorable water interaction seen in the axial region of benzene is absent.

#### B. Comparison of Different MD Simulation Conditions.

Water density maps were generated with several different water models and from simulations computed under quite different conditions (see Methods and Table 1). The water models included ENCAD's F3C and four water models implemented in GROMACS: SPC, SPC/E, TIP3P, and TIP4P. Details of the water potentials are given in Table 2, and those for the solute atoms are in Table 3. ENCAD differs significantly from GROMACS in its use of a short cutoff (6 Å) beyond which all Lennard-Jones and Coulombic interactions are zero. We sampled a wide diversity of simulation conditions to compare the results and highlight the differences and similarities in the behavior of these models.

Figure 4 shows slices of the 3-D water O and H density maps surrounding benzene computed for each set of simulation conditions. Overall, the features of these density maps are remarkably similar to each other, indicating that the dominant solute–solvent interactions are treated similarly in all of the models tested. Specifically, the position and volume of the water O density peaks above and below the benzene ring are nearly identical (Figure 4A–E). The values for the maximum  $\rho_O$  in

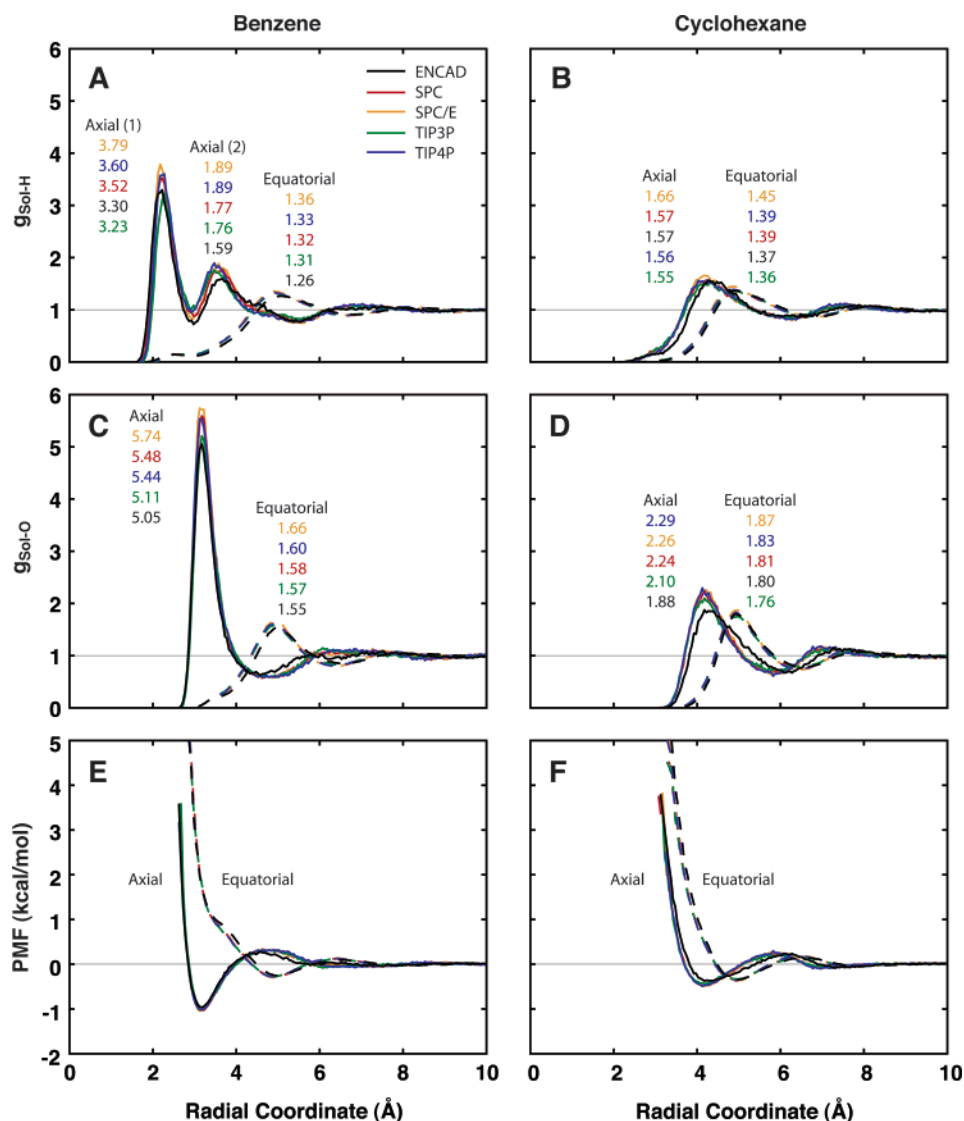


**Figure 5.** Water molecules bind strongly in the axial region surrounding benzene and weakly elsewhere. (A) The benzene centroid to water H radial distribution functions,  $g_{\text{Sol-H}}$ . The axial (solid lines) and equatorial (dashed lines) volume regions were averaged separately (see Figure 1C). Data from different simulation conditions are indicated by color: ENCAD (black), SPC (red), SPC/E (orange), TIP3P (green), TIP4P (blue). Peak heights of significant maxima are shown in the same colors for comparison. (B)  $g_{\text{Sol-H}}$  from the cyclohexane simulations. (C, D) The solute centroid to water O radial distribution functions,  $g_{\text{Sol-O}}$  for benzene and cyclohexane, respectively. (E, F) PMF, the free energy of water at varying distance from the solute center, relative to infinite separation for benzene and cyclohexane, respectively. PMF was computed from the  $g_{\text{Sol-O}}$  data shown in panels (C and D) using eq 1.  $\Delta r$  for all graphs was 0.05 Å.

these peaks vary from 5.7 (ENCAD) to 6.6 (SPC/E). The shape and intensity of the water H density in the first hydration shell are also very similar for all of the data sets (Figure 4F–J) and show a clear preference for a hydrogen-bonding interaction with the faces of the benzene ring. The maximum  $\rho_{\text{H}}$  near benzene varies from 2.9 (TIP3P) to 3.2 (TIP4P). The shape of the primary and secondary peak H density (i.e. the mushroom-shaped volume) in the ENCAD (Figure 4F), SPC (Figure 4I), and SPC/E (Figure 4J) maps is more elongated along the  $z$ -axis than for TIP4P and TIP3P (Figure 4G,H), consistent with the slightly longer O–H bond lengths in these models.

**C. Solute Center to Water Oxygen and Hydrogen Radial Distribution Functions.** While the detailed 3-D water structure maps capture many details of the hydration of benzene and cyclohexane, spatially averaged radial distribution functions are more commonly compared in the literature. Figure 5A–D show the solute center to water atom radial distribution functions,  $g_{\text{Sol-H}}$  and  $g_{\text{Sol-O}}$ , computed from each set of simulation conditions. These functions were computed for two separate volume regions as done by Linse et al.<sup>21</sup> The first is the axial

region, described by cones circumscribed by vectors at a 20° angle from the positive and negative  $z$ -axes, and the second is the equatorial region, which corresponds to the remaining volume (see Figure 1C). Partitioning the volume in this manner enhances the signal in the axial region, which is reduced by a full rotational average. The main peak heights of  $g_{\text{Sol-O}}^{\text{axial}}$  and  $g_{\text{Sol-H}}$  are dependent on the volume of the cone used for partitioning the space; selection of a narrower cone increases the peak height, while a wider cone decreases it. The position of the peak, however, is not affected by adjusting the cone volume.

The  $g_{\text{Sol-O}}$  describes the positioning of the majority of the water mass, and the results for benzene (Figure 5C) and cyclohexane (Figure 5D) can be readily compared. The main peak in the  $g_{\text{Sol-O}}^{\text{axial}}$  (solid lines) of benzene is most prominent and shows a very high density ranging from 5.05 (ENCAD) to 5.74 (SPC/E). The location of this peak is nearly identical in all of the simulation sets and is likely due to the similarity of the C–O Lennard-Jones interactions for benzene in all of the



models (Tables 2 and 3). The peak height values are notably higher than the experimentally determined peak for water, which is 3.1.<sup>40</sup> None of the models tested show a highly structured secondary peak in  $g_{\text{Sol-O}}^{\text{axial}}$ , although the ENCAD simulation (black line) shows a slight inward shift in the 5–6 Å range. The main peak in  $g_{\text{Sol-O}}^{\text{equatorial}}$  (dashed lines) for benzene is broader and weaker (peak height of 1.55–1.66) and is farther away from the benzene center (4.9–5.0 Å). In this case, the ENCAD (black dashed line) data are shifted outward slightly relative to the GROMACS simulations.

In the case of cyclohexane (Figure 5D), the differences between  $g_{\text{Sol-O}}^{\text{axial}}$  and  $g_{\text{Sol-O}}^{\text{equatorial}}$  are less pronounced. The main peak of  $g_{\text{Sol-O}}^{\text{axial}}$  is closer and higher than that of  $g_{\text{Sol-O}}^{\text{equatorial}}$ , with the exception of the ENCAD data (black line), which shows more similar heights. For cyclohexane,  $g_{\text{Sol-O}}^{\text{axial}}$  from the ENCAD simulations is shifted outward relative to the GROMACS simulations, due to the larger  $\sigma^{\text{C}}$  parameter (Table 3). One interesting observation is that the secondary peak of  $g_{\text{Sol-O}}^{\text{axial}}$  is more structured in the case of cyclohexane than for benzene. All of the cyclohexane  $g_{\text{Sol-O}}^{\text{equatorial}}$  results are comparable to each other.

The  $g_{\text{Sol-H}}$  for benzene and cyclohexane were calculated and are shown in Figure 5 (parts A and B, respectively). In all models studied, the  $g_{\text{Sol-H}}^{\text{axial}}$  data for benzene (solid lines) show two prominent peaks, indicating that the axially bound water is strongly oriented. The location of the first peak is nearly identical in all models tested, but the intensity varies from 3.23 (TIP3P) to 3.79 (SPC/E). The first peak in the H data is closer to the benzene centroid than the O peak, while the secondary H peak is slightly farther away, as expected for a hydrogen-bonding interaction. The intensity of the secondary H peak in the ENCAD simulations is shifted outward and broadened relative to the other models, perhaps due to its inherent flexibility. In contrast to  $g_{\text{Sol-H}}^{\text{axial}}$ ,  $g_{\text{Sol-H}}^{\text{equatorial}}$  is considerably less structured, with a broad, primary peak located at 4.93–5.08 Å. As with  $g_{\text{Sol-O}}$ , the  $g_{\text{Sol-H}}$  for cyclohexane (Figure 5B) shows less structure than those for benzene. The peak of  $g_{\text{Sol-H}}^{\text{axial}}$  is slightly higher and shifted inward relative to  $g_{\text{Sol-H}}^{\text{equatorial}}$  for all models studied.

**D. Energetics of Water–Solute Interactions.** The  $g_{\text{Sol-O}}$  were used to compute a radial coordinate-dependent potential of mean force (PMF) using eq 1. These results for benzene and cyclohexane are graphed in Figure 5 (parts E and F, respectively). PMF represents a free energy for the preference of water to interact with the solute at various distances from the solute centroid relative to its interaction with other water molecules in bulk. The energy of interaction in the peak in the axial volume region surrounding benzene is between –0.96 to –1.04 kcal/mol. The strongest interaction in the equatorial region is much weaker at –0.26 to –0.30 kcal/mol. For cyclohexane, the most favorable interaction energies are more equivalent in the two volume regions, with the minimum energy in the axial region between –0.38 to –0.49 kcal/mol, and that in the equatorial region between –0.34 to –0.37 kcal/mol. The outward shift of the ENCAD cyclohexane  $g_{\text{Sol-O}}$  (Figure 5D, black lines) is also seen in the PMF, but the energy values are similar to the GROMACS models.

## Discussion

In this paper, we report details of the hydration structure surrounding two cyclic hydrophobic solutes, benzene and cyclohexane, as revealed by computing spatial distribution functions of the water molecules surrounding the solutes. These 3-D hydration density maps reveal ordering in terms of the

position and orientation of the water molecules shown by the water O and H density, respectively. Most of the ordering occurs in the water molecules occupying the first hydration shell.

**A. Water Structure around Benzene.** The water molecules in the first hydration shell of benzene show a strong hydrogen bonding interaction with the faces of the benzene ring. This interaction is seen as regions of high density in the axial region of benzene (Figure 2A,B). Both the O and H density show very intense peaks directly above and below the center of the benzene ring. The H density is located closer to the benzene centroid, confirming a hydrogen bonding orientation. The other H atom is located further out than the O center, consistent with the HOH angles of the water models used, and seems to retain significant rotational freedom. From the heights of the peaks, we estimate a favorable free energy for this interaction of –1.0 kcal/mol (Figure 4F).

Our benzene water structure maps (Figures 2 and 4) are consistent with experimental studies of the hydrogen bonding of benzene with water,<sup>20,41</sup> which show that the faces of the benzene ring act as hydrogen bond acceptors. Spectroscopic experiments<sup>20</sup> place the benzene center of mass to water center of mass distance at 3.347 Å with a tilt angle of  $20 \pm 15^\circ$ , very similar to our benzene centroid to water oxygen distance of  $3.2 \pm 0.1$  Å. As with our results, the experimentally determined, preferred binding configuration has the water center of mass positioned above the center of the benzene ring.

The water structure in the equatorial region along the edge of the benzene ring (Figure 2C,D) does not show intense peaks but rather more uniform O and H density in the first hydration layer. There appears to be a subtle preference for occupying the interstices between the benzene H atoms, along the C–C bonds. The orientation of the first hydration shell waters in this region is not as obvious as in the axial region. The primary peaks in both  $g_{\text{Sol-O}}^{\text{equatorial}}$  and  $g_{\text{Sol-H}}^{\text{equatorial}}$  are more broadened than  $g_{\text{Sol-O}}^{\text{axial}}$  and  $g_{\text{Sol-H}}^{\text{axial}}$  (Figure 5A,C), and their maxima are located at about the same distance from the benzene centroid. The water density in the equatorial region is likely dominated by the allowed Lennard-Jones packing interactions, while the density in the axial region is enhanced due to more favorable Coulombic interactions.

The results reported here are comparable to previous theoretical studies of benzene hydration. Most notably, the radial distribution functions can be directly compared to  $g_{\text{Sol-O}}$  reported previously in the literature. Linse,<sup>23</sup> who used an empirically derived quantum-based potential and TIP4P water in his simulations, obtained a full rotationally averaged  $g_{\text{Sol-O}}$  that is shifted inward on the radial coordinate by about 0.4 Å relative to our  $g_{\text{Sol-O}}^{\text{equatorial}}$ . In addition, the  $g_{\text{Sol-O}}$  peak heights from that work correlate nicely with our results. The  $g_{\text{Sol-O}}$  reported by Ravishanker et al.<sup>22</sup> is also shifted inward relative to our results, and the main peak in the first hydration shell is much more intense, with a maximum peak height greater than 2.8. This result seems to indicate that the quantum-based potential used in their work included a relatively stronger benzene water interaction than in the potentials used here. The  $g_{\text{CO}}$  reported by Laaksonen et al.<sup>24</sup> is an average computed over the centers of the six C atoms, as opposed to the benzene center, and is not as easily compared to our results, but their first hydration shell peak intensity is less than 1.0 and lower than the comparable  $g_{\text{Sol-O}}$  reported by Ravishanker et al.<sup>22</sup> Jorgensen and Severance<sup>42</sup> report an optimized water benzene structure with a ring center to oxygen distance of 3.11 Å.

An interesting observation in the benzene hydration literature is that the preferred binding mode of water to the benzene ring

**TABLE 4: Comparison of Select Solute C–Water Interactions for the Different Simulations**

property <sup>a</sup>	solute	F3C	SPC	SPC/E	TIP3P	TIP4P
$r_{ij}^{\text{CO}}$ (Å) at $V_{\text{LJ}}^{\text{CO}} = kT$	benzene	3.0450	3.0500	3.0500	3.0400	3.0450
	cyclohexane	3.1350	3.0200	3.0200	3.0100	3.0150
$V_{\text{LJ}}^{\text{CO}}$ min (kcal mol <sup>-1</sup> )	benzene	-0.0624	-0.1043	-0.1043	-0.1032	-0.1042
	cyclohexane	-0.0847	-0.1013	-0.1013	-0.1002	-0.1011
$r_{ij}^{\text{CO}}$ (Å) at $V_{\text{LJ}}^{\text{CO}}$ min	benzene	3.7850	3.7700	3.7700	3.7600	3.7600
	cyclohexane	3.8300	3.7400	3.7400	3.7350	3.7350
$V_{\text{C}}^{\text{CH}}$ (kcal mol <sup>-1</sup> ) at $V_{\text{LJ}}^{\text{CO}}$ min	benzene	-0.5834	-4.1530	-4.2928	-4.2351	-5.2812
	cyclohexane	-1.1066	-4.3683	-4.5154	-4.4489	-5.5477
$V_{\text{C}}^{\text{CH}}$ (kcal mol <sup>-1</sup> ) at $V_{\text{LJ}}^{\text{CO}} = kT$	benzene	-1.2906	-5.1334	-5.3062	-5.2382	-6.5213
	cyclohexane	-2.3566	-5.4098	-5.5919	-5.5204	-6.8726

<sup>a</sup> For atom types X and Y,  $r_{ij}^{\text{XY}}$  is the Lennard-Jones distance,  $V_{\text{LJ}}^{\text{XY}}$  is the Lennard Jones energy value, and  $V_{\text{C}}^{\text{XY}}$  is the Coulombic energy value. All values were computed as described in Table 2, including the appropriate scaling of the ENCAD potentials.

is sometimes with the water oxygen centered above the benzene ring<sup>20,34</sup> and in other cases with the water oxygen positioned off of the *z*-axis and above the individual carbon atoms.<sup>24,43</sup> The benzene hydration maps presented in this paper show that the optimal binding mode is with the water oxygen centered on the benzene ring in all of the simulation conditions studied. The water molecules in our simulations form the most favorable interactions when centered between all six partial negative charges. Spatial distribution functions reported by Laaksonen et al.<sup>24</sup> show a binding energy surface with a more dispersed minimum, where water prefers to occupy positions above each carbon atom. This result is also seen in the calculations of Augsburg et al.,<sup>43</sup> who comment that the energy surface for water binding along the faces of the benzene ring is broad and relatively flat. The tendency to see one result or the other is likely linked to the fine details of the potential energy functions used in the calculation, although we note that all five different potentials used here agree on this aspect of the distribution.

**B. Water Structure around Cyclohexane.** We computed hydration maps of cyclohexane for comparison to the maps of benzene. Cyclohexane was chosen because its size and shape are similar to benzene, yet it lacks any aromaticity. Our rationale was that cyclohexane would serve as a “generic” hydrophobic solute and allow us to separate the aromatic interactions in benzene from the purely hydrophobic interactions in the case of cyclohexane. The first hydration shell of cyclohexane (Figure 3) has a water O density that is more uniform than that of benzene, with a maximum  $\rho = 2.3$  in the axial region, compared with  $\rho = 5.0$ – $5.7$  for benzene. The features of the 3-D H density maps of cyclohexane are more subtle, with slight preference for the interstices between the H atoms. Overall, the water density in the first hydration shell is comparable to that along the edge of the benzene ring. This result implies that the edges of the benzene ring are acting as a relatively general hydrophobic solute, but its solubility is increased by the favorable interactions with one water molecule hydrogen bonding to each of its faces.

Based on our results, it appears that much of the ordering in the first hydration layer surrounding cyclohexane is predominately due to the Lennard-Jones interactions between the solute and solvent. The waters in the first hydration shell of cyclohexane and in the equatorial region around benzene appear to maintain some amount of rotational freedom and do not obviously prefer to point either inward or outward (based on comparing the O and H density patterns). The maximum O density in the first hydration shell of cyclohexane is significantly lower than the primary peak in the water  $g_{\text{OO}}$  for all of the models studied. In contrast, the high density peaks in the case of benzene are most likely due to favorable electrostatic interactions.

### C. Comparison of Different Solute and Solvent Models.

In Figures 4 and 5, we compare the results of two different

MD simulation conditions, two sets of solute parameters, and five different water models. Most striking is the similarity observed between all of the different conditions. The volumes corresponding to the first hydration shell are nearly identical in all cases (Figure 4). The radial distribution functions (Figure 5A–D) also show significant similarity between the different models. In general, the largest differences occur between the ENCAD simulations and the GROMACS simulations.

It is especially noteworthy that the SPC, SPC/E, TIP3P, and TIP4P water models show nearly identical water density maps and radial distribution functions. These four models have all been parametrized to approximate different aspects of bulk water structure. For example, SPC shows a nice correlation to the experimental  $g_{\text{OO}}$  for water (including a nicely structured second peak) but has too high of a diffusion constant, too low a density, and too high a dimerization energy.<sup>29</sup> The density and diffusion constant were improved in the SPC/E parametrization.<sup>30</sup> TIP3P, on the other hand, has a higher density and diffusion constant than SPC but shows a lack of tetrahedral water structure as shown by the lack of a defined second peak in its  $g_{\text{OO}}$ .<sup>31</sup> This lack of structure was improved in the TIP4P water model, which is the only 4-point model used in this study.<sup>31</sup> TIP4P has an accurate density and lower diffusion constant. The  $g_{\text{OO}}$  for TIP4P has a well-defined second peak, but the entire function is shifted inward slightly. All of these models have a primary peak in  $g_{\text{OO}}$  that is too close and too high relative to experimental measurements. In our 3-D water density maps (Figure 4),  $g_{\text{Sol-O}}$  and  $g_{\text{Sol-H}}$  (Figure 5A–D), SPC, SPC/E, and TIP4P show the highest peak intensities, most notably in the axial region of benzene. There is evidence of the SPC and SPC/E longer OH bond length in the H density map (Figure 4H) and  $g_{\text{Sol-H}}^{\text{axial}}$  (Figure 5A). Table 4 shows a few computed interaction energies for the different solute–solvent interactions. The  $r_{\text{CO}}$  for the benzene–water interactions at  $V_{\text{LJ}} = kT$  and also the minimum  $V_{\text{LJ}}$  are very similar for all models studied. The  $V_{\text{C}}^{\text{CH}}$  at that same  $r_{\text{CO}}$  for TIP4P is significantly larger than the other models studied and is likely the cause of high peak density for that water model and for its enhanced structure in the second hydration shell (Figure 4B).

F3C is the water model primarily used in ENCAD,<sup>28</sup> and it has some notable differences from the GROMACS water models, namely the following: (1) F3C is a fully flexible model and the others were restrained to fixed bond lengths and angles, and (2) F3C includes Lennard-Jones interactions on the water H atoms while the others do not. Another significant difference is the short cutoff used for the nonbonded interactions in ENCAD. The Coulombic and Lennard-Jones interactions are all smoothly truncated to zero at 6 Å using the schemes described in Table 2. The  $r_{\text{CO}}$  for the benzene–water O interaction in ENCAD at  $V_{\text{LJ}} = kT$  (Table 4) are essentially



identical to the GROMACS models. A key difference is that the radius of the cyclohexane C is a bit larger than the other models, and this is reflected in a slight outward shift of the  $g_{\text{Sol-O}}$  and  $g_{\text{Sol-H}}$  for the ENCAD data (Figure 5B,D). The short cutoff has a much larger effect on the magnitude of the Coulombic solute-solvent interactions, which are significantly reduced in the ENCAD simulations (Table 4). This reduction does not greatly affect the water structure properties measured in our studies, however, due to the special nature of the ENCAD F3C shifting function. Although F3C has very different Coulombic interactions between pairs of atoms, the interactions between groups are almost completely unaffected by the short cutoff.<sup>28</sup>

A key conclusion from our study is that very different models, which have been calibrated to fit a variety of bulk water properties, all behave very similarly, even at the high resolution of our detailed 3-D density maps. Clearly all of these water models are appropriate for simulating the hydrophobic effect of systems at this high resolution.

**D. Conclusions.** In this paper we present detailed 3-D water structure maps surrounding two simple hydrophobic solutes. The water structure surrounding cyclohexane shows high density in the first hydration shell but little orientation preference. The edge of the benzene ring shows very similar patterns of water structure as cyclohexane and in this region acts as a conventional hydrophobic solute. The faces of benzene are very different due to the localized negative charge; each face acts as a hydrogen bond acceptor for a water molecule, greatly enhancing benzene's solubility. Comparing the results of simulations using both ENCAD and OPLS parameters for the solute and F3C, SPC, SPC/E, TIP3P, and TIP4P models for the water shows that detailed hydration patterns are remarkably similar in all cases. Even the very short nonbonded cutoff used in ENCAD models the water structure well.

**Acknowledgment.** The authors thank Patrice Koehl for the use of his "bestfit" subroutine, many helpful discussions, and critical reading of the manuscript. Thanks also to Erik Lindahl for help with GROMACS and to Rachel Kolodny for helpful discussions. This work was funded by the National Institutes of Health Grant GM-41455 (to M.L.). T.M.R. was supported by fellowship DRG-1575 from the Damon Runyon Cancer Research Foundation.

## References and Notes

- (1) Kauzmann, W. *Adv. Prot. Chem.* **1959**, *14*, 1-63.
- (2) Tanford, C. *The Hydrophobic Effect: Formation of Micelles and Biological Membranes*, Second Edition; Wiley: New York, 1980.
- (3) Israelachvili, J. N.; Marcelja, S.; Horn, R. G. *Quart. Rev. Biophys.* **1980**, *13*, 121-200.
- (4) Frank, H. S.; Evans, M. W. *J. Chem. Phys.* **1945**, *13*, 507-532.
- (5) Ben-Naim, A. *Hydrophobic Interactions*; Plenum Press: New York, 1980.
- (6) Blokzijl, W.; Engberts, J. B. F. *N. Angew. Chem., Int. Ed. Engl.* **1993**, *32*, 1545-1579.
- (7) Muller, N. *Acc. Chem. Res.* **1990**, *23*, 23-28.
- (8) Lee, B. *Biopolymers* **1985**, *24*, 813-823.
- (9) Soda, K. *J. Phys. Soc. Jpn.* **1989**, *58*, 8643-4649.
- (10) Lee, B. *Biopolymers* **1991**, *31*, 993-1008.
- (11) Soda, K. *J. Phys. Soc. Jpn.* **1993**, *62*, 1782-1793.
- (12) Eisenberg, D.; MacLachlan, A. D. *Nature* **1986**, *319*, 199-203.
- (13) Ooi, T.; Oobatake, M.; Nemethy, G.; Sheraga, H. A. *Proc. Natl. Acad. Sci. U.S.A.* **1987**, *84*, 3086-3090.
- (14) Sitkoff, D.; Sharp, K.; Honig, B. *Biophys. Chem.* **1994**, *51*, 397-409.
- (15) Simonson, T.; Brunger, A. T. *J. Phys. Chem.* **1994**, *98*, 4683-4694.
- (16) Wallqvist, A.; Covell, D. G. *J. Phys. Chem.* **1995**, *99*, 13118-13125.
- (17) Pratt, L. R. *Annu. Rev. Phys. Chem.* **2002**, *53*, 409-436.
- (18) Levitt, M.; Perutz, M. F. *J. Mol. Biol.* **1988**, *201*, 751-754.
- (19) Burley, S. K.; Petsko, G. A. *FEBS Lett.* **1986**, *203*, 139-143.
- (20) Suzuki, S.; Green, P. G.; Bumgarner, R. E.; Dasgupta, S.; Goddard, W. A., III; Blake, G. A. *Science* **1992**, *257*, 942-945.
- (21) Linse, P.; Karlstrom, G.; Jonsson, B. *J. Am. Chem. Soc.* **1984**, *106*, 4096-4102.
- (22) Ravishanker, G.; Mehrotra, P. K.; Mezei, M.; Beveridge, D. L. *J. Am. Chem. Soc.* **1984**, *106*, 4102-4108.
- (23) Linse, P. *J. Am. Chem. Soc.* **1990**, *112*, 1744-1750.
- (24) Laaksonen, A.; Stilbs, P.; Wasylishen, R. E. *J. Chem. Phys.* **1998**, *108*, 455-468.
- (25) Eisenhaber, F.; Lijnzaad, P.; Argos, P.; Sander, C.; Scharf, M. *J. Comput. Chem.* **1995**, *16*, 273-284.
- (26) Kusalik, P. G.; Svishchev, I. M. *Science* **1994**, *5176*, 1219-1221.
- (27) Svishchev, I. M.; Kusalik, P. G. *J. Chem. Phys.* **1993**, *99*, 3049-3058.
- (28) Levitt, M.; Hirshberg, M.; Sharon, R.; Laidig, K. E.; Daggett, V. *J. Phys. Chem. B* **1997**, *101*, 5051-5061.
- (29) Berendsen, H. J. C.; Postma, J. P. M.; von Gunsteren, W. F.; Hermans, J. *Intermolecular Forces*; Reidel: Dordrecht, Holland, 1981.
- (30) Berendsen, H. J. C.; Grigera, J. R.; Straatsma, T. P. *J. Phys. Chem.* **1987**, *91*, 6269-6271.
- (31) Jorgensen, W. L.; Chandrasekhar, J.; Madura, J. D.; Impey, R. W.; Klein, M. L. *J. Chem. Phys.* **1979**, *79*, 926-935.
- (32) Levitt, M. *J. Mol. Biol.* **1983**, *168*, 595-620.
- (33) Lindahl, E.; Hess, B.; van der Spoel, D. *J. Mol. Model.* **2001**, *7*, 306-317.
- (34) Jorgensen, W. L.; Maxwell, D. S.; TiradoRives, J. *J. Am. Chem. Soc.* **1996**, *118*, 11225-11236.
- (35) Allen, M. P.; Tildesley, D. J. *Computer Simulation of Liquids*; Oxford University Press: New York, 1987.
- (36) Levitt, M.; Hirshberg, M.; Sharon, R.; Daggett, V. *Comput. Phys. Commun.* **1995**, *91*, 215-231.
- (37) Essman, U.; Perera, L.; Berkowitz, M. L.; Darden, T.; Lee, H.; Pedersen, L. G. *J. Chem. Phys.* **1995**, *103*, 8577-8593.
- (38) Berendsen, H. J. C.; Postma, J. P. M.; van Gunsteren, W. F.; Dinola, A.; Haak, J. R. *J. Chem. Phys.* **1984**, *81*, 3684-3690.
- (39) McLachlan, A. D. *J. Mol. Biol.* **1979**, *128*, 49-79.
- (40) Soper, A. K.; Phillips, M. G. *Chem. Phys.* **1986**, *107*, 47-60.
- (41) Atwood, J. L.; Hamdada, F.; Robinson, K. D.; Orr, G. W.; Vincent, R. L. *Nature* **1991**, *349*, 683-684.
- (42) Jorgensen, W. L.; Severance, D. L. *J. Am. Chem. Soc.* **1990**, *112*, 4768-4774.
- (43) Augspurger, J. D.; Dykstra, C. E.; Zwier, T. S. *J. Phys. Chem.* **1992**, *96*, 7252-7257.